A Study of Microstructure in an Alloy 182/ Low Alloy Steel Dissimilar Weld Joint

J. Hou[a,b], Q.J. Peng[a], J. Kuniya[a], T.Shoji[a]
[a] Fracture and Reliability Research Institute (FRI), Tohoku University, Sendai, Japan
[b] Institute of Metal Research, Chinese Academy of Sciences, Shenyang, China

The chemical composition, hardness, characterization of microstructure in fusion boundary region of dissimilar welds between SQV2AQ low alloy steel and INCONEL Alloy 182 were evaluated. It was found that microstructure and composition transition region existed across the fusion boundary region. Composite carbide and Cr-carbide was observed, and martensite laths existed in both sides of the fusion boundary.

Keywords: Dissimilar weld joint; Fusion boundary; Type II boundary; EBSD; TEM

1. Introduction

Alloy 182 is used frequently as filler metal in the manufacture of dissimilar metal welds in light water reactors (LWR) to join the low-alloy steel (LAS) reactor pressure vessel and pressure vessel nozzles to both nickel-base wrought alloy and austenitic stainless steel components [1]. The Alloy 182, however, has been found susceptible to stress corrosion cracking (SCC) in high temperature water and concerns have been raised in recent years on the integrity of the Alloy 182-LAS dissimilar weld joint in LWR [2-6]. Investigations on the SCC behavior at the fusion boundary region of an Alloy 182-LAS dissimilar weld joint in high temperature oxygenated water have revealed that, depending on the environmental conditions and the microstructure of the fusion boundary region, an intergranular SCC crack propagated to the fusion boundary in the weld metal could exhibit three behaviors once it reached at the fusion boundary: 1) it was arrested by the fusion boundary, 2) it deflected and continued propagation along the fusion boundary, and 3) it penetrated the fusion boundary and propagated further in the base metal [7, 8]. These discoveries designate the importance of the fusion boundary microstructure in the SCC behavior of the dissimilar weld joint.

The microstructure in the fusion boundary region was investigated by transmission electron microscopy (TEM) and electron backscatter diffraction (EBSD) equipped to scanning electron microscopy (SEM). The mechanical property of the transition zone was characterized by the measurement of microhardness. The implications of the microstructure to the SCC behavior at the fusion boundary region were discussed.

2. Experiment

The dissimilar weld joint of Alloy 182- SQV2AQ LAS was prepared by multi-pass shielded metal arc welding followed by PWHT at 615°C for 25 hrs under air cooling to relieve the residual stress. Chemical compositions of both metals were shown in Table 1.

Metallographic microstructure of the weld joint was characterized by SEM following etching the specimen using a solution of $CuCl_2 \cdot 2H_2O$ (10g) + HCl (50ml) + ethonal (50ml). Micro-hardness was measured using a SHIMADZU HMV micro hardness tester with a focus on the hardness profiles across the fusion boundary region. The load and holding time used for the measurement is 10g and 20s, respectively.

Orientations and residual strain distribution in the region were analyzed using EBSD at an accelerate voltage of 25KV and a beam current of 15μA. The grain size was much smaller in LAS, so the EBSD scanning was conducted with 0.2μm step size in LAS side and 1.5μm in Alloy 182 under different magnification. The specimen for EBSD was polished by emery papers up to 4000 grit, then by diamond paste of 3μm (8min), 1μm(10min), 0.25μm (18min) and 0.1μm (30min). At last the specimen was polished using 0.02μm colloidal silica for 1 hour that provided flat surfaces with little surface deformation.

A Hitachi HF-2000 TEM was used for analyzing the crystal microstructure and precipitations. Two specimens were prepared for TEM using a Hitachi FB200A Focused Ion Beam (FIB) system. Locations of interests were identified using the scanning ion microscope attached with the FIB system. Then they were deposited by W, followed by rough cutting and fine thinning by Ga ion with different beam currents to obtain a specimen thickness of less than 100 nm. An accelerated beam voltage of 200kV was used for the TEM analyses.

3. Results and Discussion

The Alloy 182 was composed of columnar grains in dilution zone and the grains in heat affected zone (HAZ) in LAS were smaller and some laths martensite grains could be seen near the fusion boundary, Fig.1 (a). The type II boundary characteristic of dissimilar joints was observed parallel to fusion boundary about 30μm away in Alloy 182 side. A chemical composition gradient was observed from the EDX results across the fusion boundary region, Fig.1 (b). The distinct chemical composition gradient would promote martensitic and austenitic plus martensitic microstructures and results in a localized martensitic band along the fusion boundary, which may generate structure mismatch, higher hardness and higher susceptibility to cracking[9]. Typical hardness profiles were measured (Fig.1 (c)). The hardness at fusion boundary and type II boundary was much higher. The higher hardness in the narrow zone could primarily be caused by the structure mismatch and chemical composition gradient, confirmed the formation of harder micro constituents-martensite or carbides owing to the carbon migration from the LAS side[10]. A dip in hardness was noticed close to the fusion boundary in HAZ side, which was due to the depletion of carbon in this location. The increased hardness in HAZ was due to the tempered martensitic structure that developed during welding[11].

EBSD scanning was conducted in dilution zone in Alloy 182 and 13 regions of HAZ with increasing distance from the fusion boundary. The orientation maps of dilution zone and 6 HAZ regions were shown in Fig.2 (a) under different magnification. The crystal structures were B.C.C. ferrite in LAS and F.C.C. in Alloy 182, respectively. The dendritic grains with bigger size in Alloy 182 were characteristic of weld metals. The presence of small equiaxed grains along the fusion boundary and type II boundary was observed. The morphology of these grains resembled the appearance of a "chill zone" in a large casting where equiaxed grains nucleate randomly along the mold wall[12]. The equiaxed grains were not grown epitaxially from the LAS. Misorientation analyses were conducted between HAZ and weld metal grains along the fusion boundary, large-angle grain boundary misorientations were exhibited with trend in preferred misorientation of K-S, N-W and Bain relationships between HAZ and weld metal grains, unlike the random distribution of grain boundary misorientations in Type 409/Monel system[12]. The orientation relationships were defined by specifying the angle and axis of rotation necessary to align these planes and directions. As the angle pairs for the Bain, K-S, N-W orientation relationships are approximately 45 deg @<100>, and 35 deg @<110> and 45 deg @<110>, respectively. Morito et. al. researched the crystal microstructures of Fe-C alloys and concluded

Table 1: Chemical compositions of base and weld metals (wt %).

Element	C	Si	Mn	P	S	Cu	Ni	Cr	Mo	V	NbTa	Nb	Ti	Fe
Low Alloy Steel	0.20	0.24	1.42	0.01	0.006	0.11	0.64	0.12	0.54	0.003		0.002	0.001	Bal.
Alloy 182	0.053	0.44	6.50	0.004	0.002		68.90	14.7			1.55	1.50		7.23

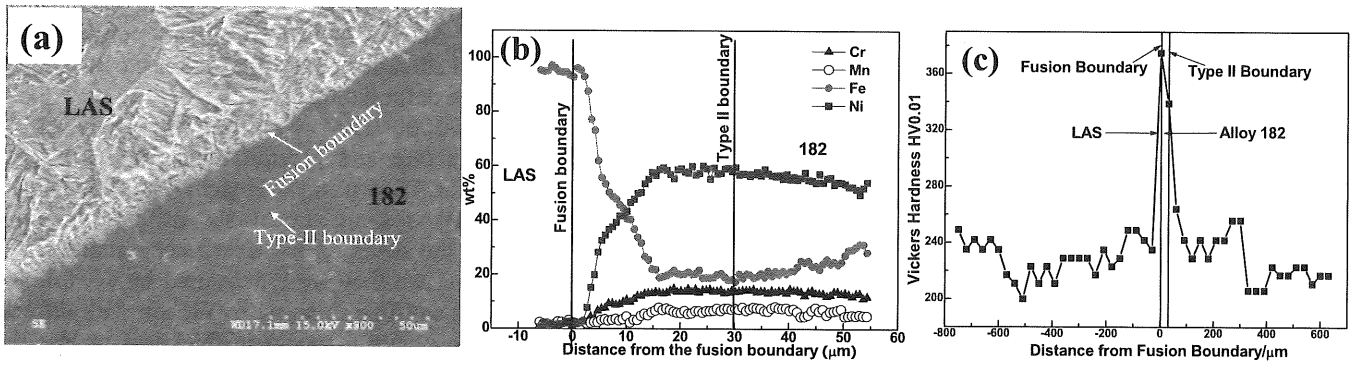

Fig.1 The region across the fusion boundary and type II boundary: (a) SEM micrograph, (b) composition profiles across the fusion and Type II boundary,(c) typical micro hardness profile across the fusion and type II boundary.

that the parent austenite grains and produced ferrous grains were with the relationships of: the parent grain was divided into packets (the group of laths with same habit plane) and each packet was further subdivided into blocks (the group of laths with same orientation) [13-16]. The colored maps in HAZ indicated that the packets were obvious and with bigger size in the regions nearer the fusion boundary (about 300μm distance). In each packet, there were three blocks with different orientation. In each block, the laths orientation was similar with small misorientation, which was denoted as sub-block [13,17]. With the increasing distance from the fusion boundary, blocks were finer and more degenerate, while the presence of sub-block was still recognizable. That was maybe because that the regions nearer the fusion boundary were C-depleted because of carbon diffusion from LAS to Alloy 182 comparing to the regions with bigger distance, the increased C content would decreased the block size. The misorientation distribution of the regions in HAZ was measured and shown in Fig.2 (b), and the regions were marked as 1 to 13. The angles smaller than 5° were not represented in the profiles, because they never corresponded to a packet boundary. The strong peak at the misorientation angle of around θ=60°, together with analysis of the individual axis angle pairs corresponding to the packet boundaries, showed that most of the packets were in fact twin related, the axis angle pair describing the misorientation relationship being $60°<111>_{\alpha}$ [13,17]. The peaks at around 53-54° were interpreted according to previous works. This misorientation angle and the corresponding axis pairs could be best accounted for assuming (near) NW/NW misorientation relationships. This suggests that in HAZ regions during the welding, packets were grown with KS and near NW relationships. The EBSD technique had been applied to studies concerned with deformation mechanism and strain measurements.

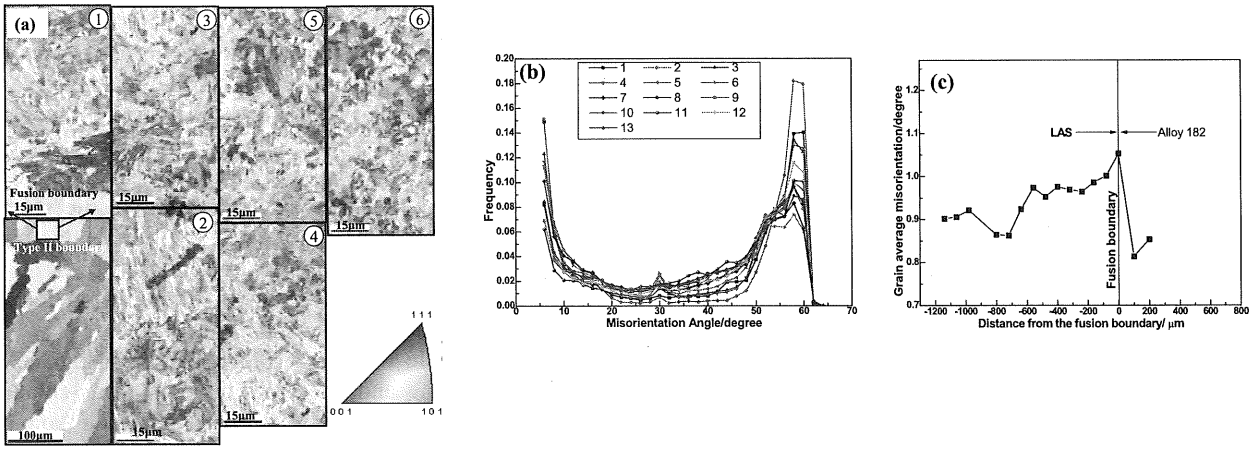

Fig.2 EBSD results of the HAZ obtained from 13 regions (a) orientation maps of 6 regions; (b) the histograms of misorientation angle distributions obtained from these 13 regions; (c) the average intra-grain misorientation profile.

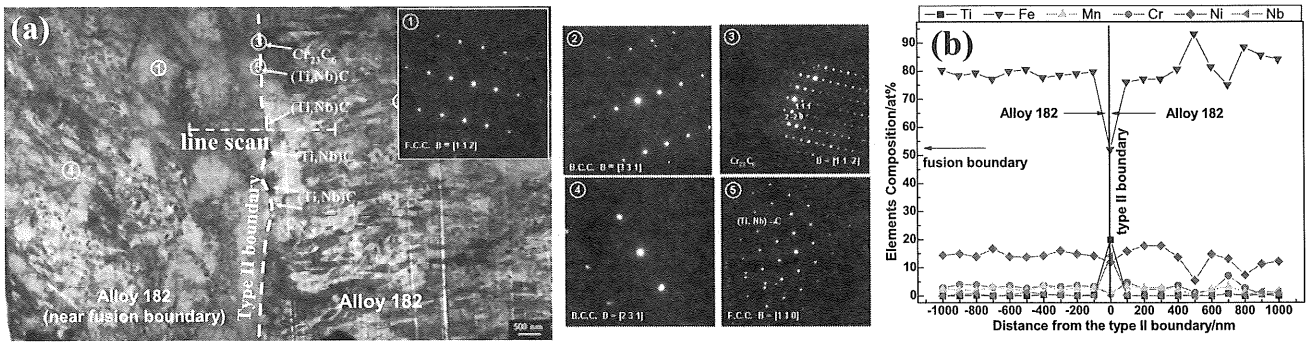

Fig. 3 TEM observation of the specimen 1: (a) image of the region across type II boundary; (b) TEM-EDX analysis line scanning across the type II boundary.

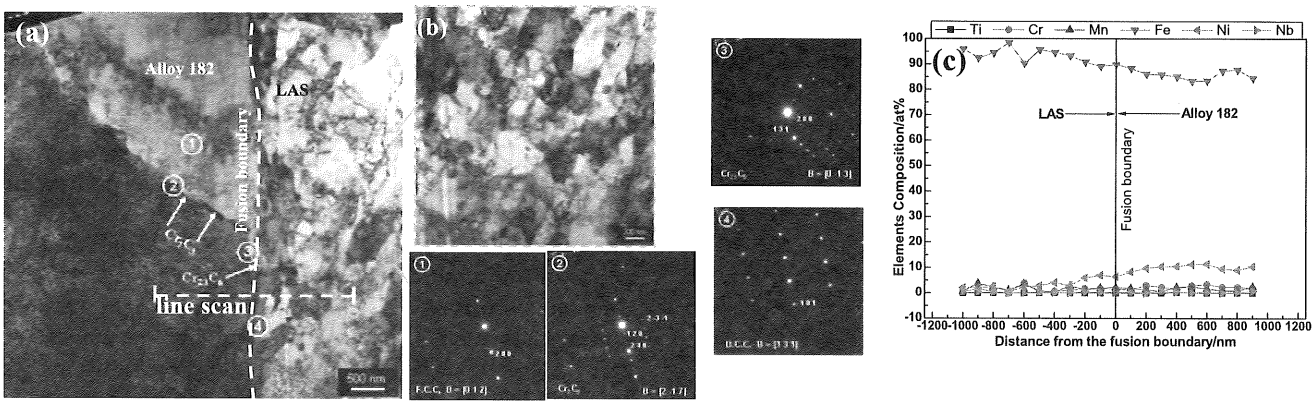

Fig. 4 TEM observation of the specimen 2: (a) image of the region containing the fusion boundary and grain boundary; (b) high magnification image of the cyan-dashed frame; (c) TEM-EDX analysis line scanning across the fusion boundary.

The intra-grain misorientation was used to estimate the internal rotation within a given grain due to plastic deformation[18, 19]. In this work, the intra-grain average misorientation (GAM) was applied to qualitatively estimate the residual strain distribution in the HAZ region. The residual strain estimated by GAM was just the intra-grain strains, extracting the influence of grain boundary. The highest levels of GAM was observed in the region closest to the fusion boundary, with the sub-structure decreasing to a minimum at about 700 μm from the fusion boundary (Fig.2 (c)). The sub-structure increased slightly and to a much smaller value out to about 1200 μm. Some scratches and inclusions were observed in the electron backscattered images near 800 μm and therefore some of this slight increase may be artificial.

The morphology of type II boundary was observed by high magnified TEM (Fig.3 (a)). The left side was the region nearer the fusion boundary. The diffraction patterns ①, ② and ④were taken in the positions in both sides of the type II boundary, indicating the mixed existence of grains with B.C.C. ferritic/martensitic and F.C.C. austenitic structure. The small size laths martensite was observed clearly in both sides (diffraction pattern), coexisting with big size austenite grains. The orientation relationship between them was mainly K-S and N-W relationship ({111}fcc//{110}α) [20]. Obvious discontinuous precipitations were observed along the type II boundary. From the results of diffraction pattern (③ and ⑤), EDS spot and line scanning (Fig. 2 (b)), it could be identified that the dominant precipitation was composite carbide of Ti and Nb. In addition, the Cr-carbide $Cr_{23}C_6$ was also observed. According to the diffraction pattern, there was no certain relationship between the orientations of precipitations and boundary. The Fe element composition was very high in the Alloy 182, indicating the migration from LAS to Alloy 182 in the regions near the fusion and type II boundary. Even though the carbon content was not assessed in this region, the microstructural observations discussed earlier clearly suggest the migration of carbon from the relatively carbon rich LAS into the weld metal region. The above conditions would have facilitated, synergistically, the development of a martensitic structure and formation of carbides in the region closer to the type II boundary, leading to higher hardness.

Fig.4 showed the TEM observation of the fusion boundary and grain boundary. In the image, the left side was Alloy 182 and right side was LAS (Fig.4 (a)). In Alloy 182, the grain size was big and one grain boundary was contained. Precipitations could be observed on the grain boundary. According to the inserted diffraction patterns ① and ②, the orientation relationship between grain boundary precipitation and matrix was (200) layer parallel to (120) layer of matrix. The precipitations on grain boundary could be identified as Cr_7C_3 according to the diffraction pattern and EDX. At the joint of grain boundary and fusion boundary, the $Cr_{23}C_6$ precipitation was observed. No carbide precipitation was observed on fusion boundary. The mapping results of the region across the grain boundary and fusion boundary showed that the Mn element was enriched distributed along the fusion boundary and in the regions of LAS. The high magnification image of the cyan-dashed frame showed obvious laths martensite in LAS, Fig.4 (b). The result of EDX line scanning across the fusion boundary indicated that from the LAS side to Alloy 182, the Fe element composition decreased slightly, however, it was still much higher than the matrix Alloy 182, which indicating the diffusion of Fe to Alloy 182 in regions near the fusion boundary. The grains in Alloy 182 were with F.C.C. structure, bigger size and high Fe composition.

4. Conclusions:

The crystallographic microstructure, chemical composition, orientation relationship and residual stress distribution in dissimilar metal weld joint between low alloy steel and nickel base alloy were studied. The following conclusions can be drawn.

(1) The crystallographic microstructure and chemical composition transition region was existed across the fusion and type II boundary. Mixed structure of austenite and martensite was observed in transition region.

(2) The fusion boundary and type II boundary had the highest hardness. Residual strain distribution in HAZ was higher and decreased with increasing distance from the fusion boundary.

(3) The orientation relationship between laths martensite and austenite was K-S, N-W and Bain relationship.

(4) Lots of composite carbides of Ti and Nb and some $Cr_{23}C_6$ were observed on type II boundary. On fusion boundary, little carbide was observed while some martensite laths were existed. Some Cr_7C_3 and $Cr_{23}C_6$ were observed on grain boundary near the fusion boundary in Alloy 182.

5. Acknowledgements:

This work was performed as a part of "SCC mechanism studies of the Fusion Boundary Region of Ni base weld metal and Low Alloy Steel Dissimilar Weld Joint in High Temperature Oxygenated Water" organized by JSCE and sponsored by Japanese BWR utilities and partially by The Special Funds for the Major State Basic Research Projects G2006CB605000 (973 Program, China).

References

[1] M. Sireesha, S. K. Albert, V. Shankar, S. Sundaresan, Journal of Nuclear Materials 279 (2000) 65-76.

[2] USNRC, Recent Experience with Degradation of Reactor Pressure Vessel Head, in: USNRC, Information Notice 2002-11, 12 March 2002.

[3] USNRC, Crack in Weld Area of Reactor Coolant System Hot Leg Piping at V.C. Summer, in: USNRC Information Notice 2000-17, 18 October 2000.

[4] G. E. M. J.I. Bennetch, L.L. Spain, G.V. Rao, Service Experience and Failure Assessment Applications ASME 2002, ASME PVP, New York, 2002, p. 179-185.

[5] Q. Peng, T. Shoji, H. Yamauchi, Y. Takeda, Corrosion Science 49 (2007) 2767-2780.

[6] P. L. Andresen, J. Hickling, A. Ahluwalia, J. Wilson, Corrosion 64 (2008) 707-720.

[7] H. P. Seifert, S. Ritter, T. Shoji, Q. J. Peng, Y. Takeda, Z. P. Lu, Journal of Nuclear Materials 378 (2008) 197-210.

[8] Q. Peng, T. Shoji, S. Ritter, H.-P. Seifert, in: P. J. K. T.R. Allen, and L. Nelson, (Ed.) 12th International Conference on Environmental Degradation of Materials in Nuclear Power System – Water Reactors, TMS 2005, pp. 589-599.

[9] M. D. Rowe, T. W. Nelson, J. C. Lippold, Welding Journal 78 (1999) 31S-37S.

[10] P. B. Srinivasan, V. Muthupandi, W. Dietzel, V. Sivan, Materials & Design 27 (2006) 182-191.

[11] P. B. Srinivasan, V. Muthupandi, W. Dietzel, V. Sivan, Journal of Materials Engineering and Performance 15 (2006) 758-764.

[12] T. W. Nelson, J. C. Lippold, M. J. Mills, Welding Journal 78 (1999) 329S-337S.

[13] S. Morito, H. Tanaka, R. Konishi, T. Furuhara, T. Maki, Acta Materialia 51 (2003) 1789-1799.

[14] J. M. Chilton, C. J. Barton, G. R. Speich, Journal of the Iron and Steel Institute 208 (1970) 184-&.

[15] G. Krauss, A. R. Marder, Metallurgical Transactions 2 (1971) 2343-&.

[16] T. Maki, K. Tsuzaki, I. Tamura, Transactions of the Iron and Steel Institute of Japan 20 (1980) 207-214.

[17] S. Morito, X. Huang, T. Furuhara, T. Maki, N. Hansen, Acta Materialia 54 (2006) 5323-5331.

[18] L. N. Brewer, M. A. Othon, L. M. Young, T. M. Angeliu, Microscopy and Microanalysis 12 (2006) 85-91.

[19] T. M. Angeliu, P. L. Andresen, E. Hall, J. A. Sutliff, S. Sitzman, R. M. Horn, Intergranular Stress Corrosion Cracking of Unsensitized Stainless Steels in BWR Environments, in: Ninth International Symposium on Environmental Degradation of Materials in Nuclear Power Systems-Water Reactors 1999.

[20] A. F. Gourgues, H. M. Flower, T. C. Lindley, Materials Science and Technology 16 (2000) 26-40.